ACS APPLIED MATERIALS & INTERFACES

Research Article

www.acsami.org

The Influence of Deposition Solution pH and Ionic Strength on the Quality of Poly(*N*-isopropylacrylamide) Microgel-Based Thin Films and Etalons

Liang Hu and Michael J. Serpe*

Department of Chemistry, University of Alberta, Edmonton, AB, T6G 2G2 Canada

Supporting Information

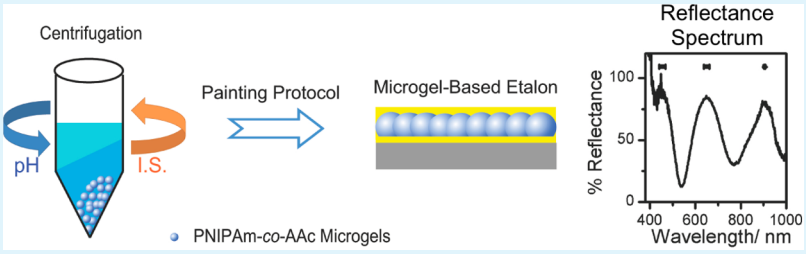

ABSTRACT: Poly(*N*-isopropylacrylamide)-*co*-acrylic acid (pNIPAm-*co*-AAc) microgel-based thin films and etalons were fabricated via "painting" a pNIPAm-*co*-AAc microgel monolayer on a Au-coated substrate, followed by the deposition of another Au overlayer. Herein, in situ observation of how the pH and ionic strength (I.S.) of the painting solution influenced microgel deposition and, ultimately, the optical homogeneity and pH sensitivity of the etalon was carried out. It was shown that microgels closely pack on the Au substrate when they are deposited at pH 3.0, leading to a good optical homogeneity. Additionally, increasing the painting solution I.S. leads to a slight decrease in microgel packing density on the substrate, but enhances the ability of the microgel layer to swell, exhibiting thicker polymer layers when immersed in pH 3.0 solutions. When painting at pH 7.5, the optical homogeneity of the etalon is improved at the expense of swellability, exaggerated high I.S. We also determined the device's sensitivity to pH changes and found a maximum sensitivity when the microgels were deposited at pH 7.5 with an I.S. of 10 mM.

KEYWORDS: *N-isopropylacrylamide, stimuli responsive polymers, thin films, microgel-based etalon, painting solution, pH sensitivity*

INTRODUCTION

Microgels are colloidally stable cross-linked polymer networks, with diameters ranging from ∼100 nm to micrometers.[1−6] Stimuli responsive microgels have been extensively studied due to their rapid tunable physical and chemical properties in response to external stimuli.[7−10] Because of their unique thermoresponsive behavior, poly(*N*-isopropylacrylamide) (pNIPAm)-based microgels have been the topic of many investigations.[8−12] Specifically, pNIPAm-based microgels are hydrophilic and highly swollen in water when the temperature of the water they are dissolved in is below pNIPAm's lower critical solution temperature (LCST) of ∼32 °C. The microgels collapse above the LCST, transitioning to a deswollen state. Importantly, the thermoresponsivity is reversible. That is, when the temperature is decreased to <LCST, the pNIPAm microgels reswell and again become fully hydrated. Additionally, functional moieties can be easily incorporated into pNIPAm microgels by simple copolymerization to provide a myriad of functionalities.[8,9,11,13,14] For example, pNIPAm-*co*-acrylic acid (pNIPAm-*co*-AAc) microgels have been conferred additional pH and ionic strength (I.S.) responsivity.[8,11,12] Briefly, at pH > pK_a for AAc (∼4.25),[15] AAc groups are deprotonated; thus, pNIPAm-*co*-AAc microgels swell due to the electrostatic repulsion force.

PNIPAm microgel-based assemblies have shown great potential for antifouling coatings,[16−18] controlled/triggered drug delivery,[19,20] water remediation,[21,22] and photonic materials.[23−25] As shown in Scheme 1, we have fabricated colored materials by sandwiching pNIPAm-based microgels between two thin semitransparent metal layers to make a so-called Fabry−Pérot etalon (or simply etalon).[23,26] When light impinges on the etalon, it enters and resonates in the microgel layer between the mirrors, leading to a constructive/destructive interference and thus visible color. Additionally, a reflectance spectrum can be collected that exhibits peaks centered at specific wavelengths, which can be predicted using the following equation

$$m\lambda = 2nd\cos\theta \quad (1)$$

where m is the peak order, λ is the wavelength maximum of the peak(s), n is the refractive index of the pNIPAm microgel layer,

Received: September 2, 2013
Accepted: October 18, 2013
Published: November 5, 2013

Scheme 1. Structure of a pNIPAm Microgel-Based Etalon[a]

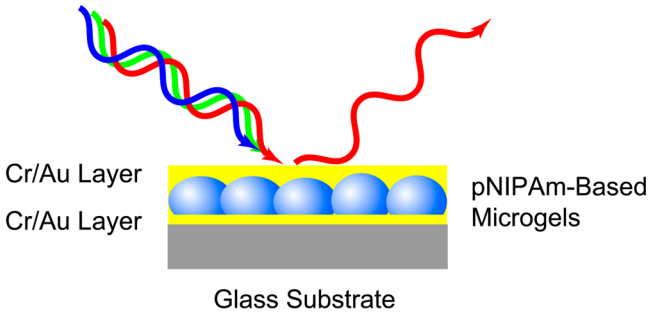

[a]Typical thicknesses for the Cr and Au layers are 2 and 15 nm, respectively.

d is the distance between two Au layers, and θ is the angle of incidence.

We have shown that pNIPAm microgel-based etalons can exhibit tunable colors, or λ, in response to external stimuli. This is mainly due to the microgel layer swelling/deswelling perpendicular to the underlying substrate, resulting in a change of the distance between the two Au mirrors (d).[23] Using this principle, we have designed pNIPAm microgel-based etalon sensors.[15,27−30]

For sensing applications, the optical homogeneity and sensitivity of etalons are of significance. To yield optically homogeneous etalons, we have developed a "painting" protocol, instead of a traditional solution drying method. The "painting" protocol is capable of yielding a monolithic, dense, and uniform microgel monolayer on a Au "mirror" coated substrate, such that a reflectance spectrum can be observed in every region above the etalon.[15,31] Furthermore, the standard deviation of the peak position obtained from many different spots on a single etalon is no more than 25 nm.[15] This standard deviation (or ideally less) in the peak position is desirable for our applications.

In a typical microgel painting procedure, the microgels dissolved in deionized (DI) water are centrifuged at high speed to pack the microgels into a dense, viscous pellet. Then, they are "painted" onto the Au surface. However, since pNIPAm-*co*-AAc microgels are both pH and ionic strength (I.S.) responsive, the water pH and ionic strength necessarily influence the intra- and intermicrogel interactions, which will affect the microgel hydrodynamic diameter, microgel−microgel interactions, and the microgel−surface interactions. Ultimately, water pH and I.S. will influence the quality of the microgel layer deposited on Au, and most importantly, the homogeneity of the optical properties of the etalon. That is, the standard deviation of the etalon's peak position will be affected. Hence, solution pH and ionic strength should be controlled to yield etalons with the most uniform and reproducible optical properties.

In this paper, we generate pNIPAm-*co*-AAc microgel solutions with a variety of pH and I.S. values. We first study how solution pH and I.S. impact the dispersed microgel hydrodynamic diameter. We then fabricate a series of microgel layers on Au coated glass substrates by painting the various solutions with different pH and I.S. on the Au. After deposition, etalons are formed by coating the microgel layer with the standard Cr/Au overlayer. The resultant microgel structure and the etalon's optical properties were investigated when immersed in pH 3.0 (I.S. 2 mM) solution using atomic force microscopy and reflectance spectroscopy, respectively. Finally, the sensitivity of the etalon in response to solution pH changes from pH 3.0 to pH 6.5 was investigated. This work will help guide our etalon fabrication efforts to generate more optically homogeneous and/or sensitive etalons, which also allows for the generation of improved sensors. *Possibly most importantly*, it sheds light on how charged colloids interact with solid substrates, and how that interaction can be mediated and controlled to yield coatings with desired properties, i.e., different morphologies, coverage, and colloid distribution.

EXPERIMENTAL SECTION

Materials. *N*-Isopropylacrylamide (NIPAm) was obtianed from TCI (Portland, Oregon) and purified by recrystallization from hexane (≥98.5 %, Sigma-Aldrich) prior to use. *N*,*N*′-Methylenebisacrylamide (BIS, 99 %), acrylic acid (AAc, 99 %), and ammonium persulfate (APS, 98 %) were obtained from Sigma-Aldrich (Oakville, Ontario). Sodium chloride and sodium hydroxide were purchased from EMD (Mississauga, Ontario). Glass substrates (25 mm × 25 mm) were obtained from Fisher (Ottawa, Ontario). Deionized (DI) water was filtered to have a resistivity of 18.2 MΩ·cm and was produced by a Milli-Q Plus system (Millipore Co.). Au (99.99 %) and Cr (99.999 %) were purchased from ESPI Company and MRCS Canada (Edmonton), respectively. Whatman #1 paper filters were obtained from GE Healthcare (U.K.).

PNIPAm-*co*-AAc Microgel Synthesis. Microgels were prepared according to the literature.[27] A three-neck round-bottom flask was fitted with a reflux condenser, a nitrogen inlet, and a temperature probe, and charged with a solution of NIPAm (11.9 mmol), BIS (0.703 mmol), and DI water (99 mL), which was previously filtered through a 0.2 μm filter. The solution was allowed to heat to 70 °C for ∼1 h while bubbling N_2 gas through the solution, followed by the addition of AAc (1.43 mmol) and a solution of APS (0.2 mmol, in 1 mL DI water) to initiate the reaction. The reaction occurred at 70 °C for 4 h under a N_2 gas atmosphere. The resulting suspension was allowed to cool overnight, and then filtered through a Whatman #1 paper filter in order to remove any large aggregates. The microgel solution was purified via centrifugation at ∼8300 rcf to form a pellet, followed by removal of the supernatant and resuspension with DI water, 6×. The as-prepared pNIPAm-*co*-AAc microgels show an LCST of ∼32 °C (see the Supporting Information).[23] To study the effect of microgel solution pH and I.S. on deposition behavior, and etalon optical properties, the microgel pellets from above were resuspended with various pH and I.S. solutions. Then, the resultant microgel solutions were centrifuged at ∼8300 rcf to form a pellet, followed by removal of the supernatant and resuspension with corresponding pH/I.S. solutions a total of 6× to ensure complete exchange of the water with the desired solution. pH solutions were made by adding either HCl for pH 3.0 or NaOH for pH 7.5 to DI water. NaCl was used to adjust the I.S. accordingly.

Substrate and Etalon Fabrication. A 25 mm × 25 mm glass substrate was first rinsed with ethanol and dried with N_2 gas. Then, 2 nm of Cr and 15 nm of Au were deposited to the glass substrate one after the other, at a rate of 1 and 0.1 Å s^{-1}, respectively, using a thermal evaporation system (Torr International Inc., New Windsor, NY). The Au-coated substrate was annealed at 250 °C for 3 h and cooled to room temperature prior to the deposition of the microgel monolayer.

PNIPAm-*co*-AAc microgel monolayers were deposited on the Au surfaces, from the respective solution above, via the "painting" protocol.[31] After coating another Cr/Au mirror on the deposited microgel monolayers, pNIPAm-*co*-AAc microgel-based etalons were obtained.

Characterization. The microgel diameter in solution was measured using an ALV/CGS-3 compact goniometer (Germany) with a HeNe laser (incident beam = 632.8 nm, scattering angle = 90°). All measurements were taken at 25 °C. Each hydrodynamic radius reported was an average diameter obtained from five measurements, each with a 30 s acquisition time.

Atomic force microscopy (AFM) was carried out with an MFP-3D (Asylum Research) in tapping mode in pH 3.0 (2 mM) solution at 25 °C. Etalons were immersed in pH 3.0 with an I.S. 2 mM solution and left for 1 h for microgel particle swelling before imaging.

Reflectance spectra were collected using a Red Tide USB650 spectrometer, and a LS-1 tungsten light, both connected to a reflectance probe (Ocean Optics, Dunedin). The spectra were collected over a wavelength range of 400−1000 nm and analyzed by Ocean Optics Spectra Suite Spectroscopy software.

RESULTS AND DISCUSSION

Microgels in Solution. Figure 1 shows the hydrodynamic radius (R_H) of pNIPAm-*co*-AAc microgels dissolved in solutions of various pH and I.S. As can be seen in Figure 1, the R_H of the microgels at high pH is always greater than that at low pH. This is due to deprotonation of the AAc groups at pH > ~4.25 (pK_a for AAc). The generated charges leads to intramicrogel Coulombic repulsion and increased osmotic pressure, which lead to microgel swelling, and hence an increase in the R_H.[32,33] Also, as can be seen in Figure 1, the R_H decreases significantly with increasing I.S. from 2 to 6 mM in pH 7.5 solution. However, R_H changes only slightly when the I.S. is further increased to 10 mM. This indicates that no excessive microgel electrostatic repulsions are shielded under an I.S. of 10 mM. Meanwhile, it is clearly shown that I.S. has little effect on R_H at pH 3.0. This is due to the fact that there is minimal charge in the microgel network at pH 3.0, although there is some due to the charged APS initiator.

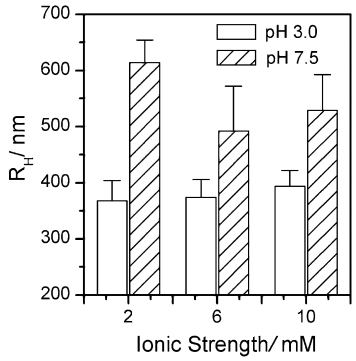

Figure 1. R_H of solution dispersed pNIPAm-*co*-AAc microgels as a function of solution pH and I.S.

Etalon Morphology in pH 3.0 Solution. Microgel monolayers were generated via painting the microgel solutions with various pH/I.S. on the Au surfaces, followed by the deposition of another Au layer via thermal evaporation to construct the etalon. Finally, the resultant microgel-based etalons were immersed in pH 3.0 solution with an I.S. of 2 mM at 30 °C overnight, ensuring that etalons were completely solvated. The surface morphology of the etalons was then determined by atomic force microscopy (AFM) imaging in pH 3.0 (2 mM I.S.) solution at 25 °C. Figure 2 shows that, when the microgel deposition solution is pH 3.0 (2 mM I.S.), pNIPAm-*co*-AAc microgels pack closely and have a large number of particles per area (particle number density), and pack fairly homogenously. To elucidate the surface morphologies in all cases, we further averaged the center-to-center distance (D_C) of the adjacent microgel particles at five random spots from these AFM images (e.g., see Figure 2b,c) and found that the D_C in this series was 487 ± 35 nm (painting solution I.S. 2 mM), 493 ± 40 nm (painting solution I.S. 6 mM), and 499 ± 59 nm (painting solution I.S. 10 mM), respectively. More details can be seen in the Supporting Information. Considering pNIPAm-*co*-AAc microgels as soft colloids,[34,35] $D_C < 2 \times R_H$ in all cases is indicative of adjacent microgel overpacking.[33,36,37] To further characterize the packing density, we averaged the microgels apparent diameter (D) on the surface of five random single microgel particles from these AFM images. The results are 542 ± 33 nm (painting solution I.S. 2 mM), 552 ± 36 nm (painting solution I.S. 6 mM), and 562 ± 23 nm (painting solution I.S. 10 mM), respectively. Although D_C and D are similar regardless of the solution I.S., we feel though that the increase in both values with increasing I.S. points toward a lower particle number density with increased I.S.

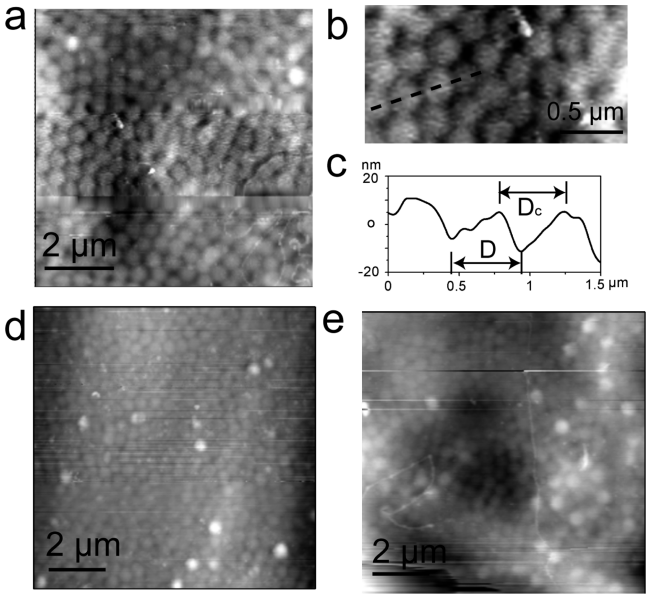

Figure 2. AFM images of pNIPAm-*co*-AAc microgel-based etalons in pH 3.0 solution (2 mM I.S.). These etalons were fabrciated from microgel deposition solutions at pH 3.0 with an I.S. of (a−c) 2, (d) 6, and (e) 10 mM. Panel (b) is the zoom of (a). Panel (c) is the cross-sectional profile of (b) defined by the line.

In our experiments, the concentration of microgels in the painting solution is extremely high, resembling a colloidal glass.[38,39] Therefore, the microgel−microgel interactions are complex and of extreme importance, mainly involving attractive interactions (inter/intramolecular hydrogen bonding, van der Waals interactions, hydrophobic interactions) and soft repulsive interactions.[39] As with microgel−microgel interactions, the interactions between the microgels and surface also play a significant role in the assembly process.[32,40,41] This is most likely a result of the strong attraction between the microgel's N and O and the Au substrate.[42,43] Therefore, the observed assembly behavior is a result of the complex interplay between microgel−microgel and microgel−surface interactions. We acknowledge that these chemical bonds could be probed by spectroscopic analysis, but unfortunately, it was difficult to get useful information possibly as a result of scattering from the dried microgels, or as a result of the large NIPAm background overpowering the signal from these less prominent bonds. Regardless, in this paper, we use in situ observation of the swelling behavior of the microgels as an alternative to understand the consequences of these bonds.

During the painting process, an excess volume (~40 μL) of a highly concentrated microgel suspension is spread on the Au surface at 30 °C; therefore, we predict that the excess microgels do not directly stick to the Au surface, and exist as layers on top of the microgels directly stuck to the Au.[31] Following the initial painting, the films are allowed to "age" for 2 h at 35 °C (> LCST of pNIPAm microgel at pH 3.0). At this temperature, the microgels deswell, making it possible for some excess microgels to penetrate between pre-adsorbed microgels and occupy the Au surface that was not previously accessible. Furthermore, in this case, the AAc groups are protonated, leaving only a slight negative charge on the microgel due to the presence of the initiator, making the microgel−microgel interactions favorable. Recently, Burmistrova et al.[32] deposited pNIPAm-*co*-AAc microgels on silicon wafers precoated with polyethylene imine (PEI). They showed that, with increasing I.S. from 0 to 10 mM, fewer microgels−PEI bonds could be formed due to counterion screening.[32] On the basis of this, we believe that, in our case, increasing I.S. also shields the microgel's N and O lone pair electrons over a certain distance and, accordingly, less microgels are attached to the Au-coated surface, leading to a decrease in packing density of the microgel layer. Hence, the assembly of the pNIPAm-*co*-AAc microgel monolayer on the Au surface is dominated by the compression and the thermal energy of the system, but is also afftected by both above-mentioned contradictive (i.e., low microgel−microgel electrostatic repulsion combined with weakened microgel−surface interactions) phenomena, leading to an overall slight decrease in the attaction of microgels for the surface at high I.S. Therefore, the etalon painted at pH 3.0 with a higher I.S. shows a lower packing density.

Likewise, we studied the influence of painting I.S. at pH 7.5 on surface morphologies of the etalon immersed in pH 3.0 (2 mM I.S.) solution. As seen in Figure 3, the particle number density increases with increasing I.S. PNIPAm-*co*-AAc microgels painted at pH 7.5 with an I.S. of 2 mM exhibit the largest D_C = 754 ± 18 nm. Surprisingly, the microgels in Figure 3b,c become "fuzzy" and exhibit large "aggregates" with increasing painting I.S., such that D_C is impossible to measure. Note that these fuzzy images are not a result of the microgels exhibiting a poor size distribution, as can be seen via differential interference contrast (DIC) microscope images; see the Supporting Information. We take this as an indication of the highest packing density and is most likely a result of the intermicrogel interactions causing the microgels to appear integrated (Figure 3d). Painting at 2 mM I.S., the assembly of microgel on the Au surface driven by microgel compression and thermal energy is frustrated by the strong Coulombic replusion and lowest electrostatic shielding, resulting in fewer microgels attached to the Au surface, and yielding the largest D_C. Increasing painting I.S. leads to a pronounced decrease in R_H (Figure 1) and more shielding of the charges inside and between the microgels. Therefore, much more microgels can be compressed, diffuse, and finally occupy on the surface, giving rise to a significant increase in the particle packing density. Additionally, as a consequence of the interruption of the microgel−Au interactions caused by higher I.S., packing density is expected to be decreased slightly, but in the regime of strong microgel−surface interactions, this has an apparent negligible effect. Again, the result in Figure 3 shows that the microgel monolayer assembles on the Au surface in pH 7.5 solution, which is induced by microgel compression and thermal energy, but also depends on the microgel−microgel interactions, which are greatly affected by I.S., and the microgel−Au interactions.

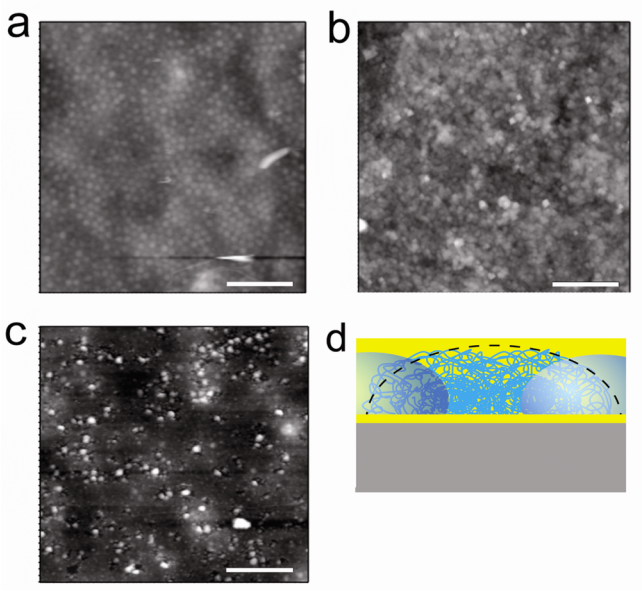

Figure 3. AFM images of pNIPAm-*co*-AAc microgel-based etalons in pH 3.0 solution (2 mM I.S.). These etalons were created from microgel deposition solutions at pH 7.5 with an I.S. of (a) 2, (b) 6, and (c) 10 mM. Scale bars are 5 μm. (d) A proposed mechanism for large "aggregates" in (c).

On the basis of the AFM data shown in Figures 2 and 3, we believe that the assembly of the pNIPAm-*co*-AAc microgel monolayer on the Au surface is driven by microgel compression and thermal energy, but two more contributions should be also considered: (1) microgel−microgel interactions and (2) microgel−surface (Au) interactions (Scheme 2).

Etalon Thickness in pH 3.0 Solution. In our previous work, we established that the visual color, and the position of the peaks in the reflectance spectra, depended on the thickness of the etalon.[23] Therefore, we measured the distance between the two Au mirrors (d) of the etalon in pH 3.0 solution (2 mM I.S.) at different microgel deposition solution pH and I.S. The etalon thickness was determined from five random regions of an AFM image of each etalon (see the Supporting Information), and shown in Figure 4. Figure 4 shows that, at pH 3.0, the etalon thickness increases with increasing deposition solution I.S. Albeit the thermal energy and compression allow protonated microgels (at pH 3.0) to assemble and pack closely on the surface, the microgel monolayer swelling can be explained by considering the microgel−microgel and microgel−Au interactions. As mentioned previously, with increasing I.S., the packing density decreases as a result of the weakened microgel−surface interactions. As shown in Scheme 2, once etalons are in pH 3.0 (2 mM I.S.) solution, new microgel−Au bonds conferred between both Au layers are formed, and the total number of interactions are directly proportional to packing density (Scheme 2). Also, at 2 mM, the Debye screening length is so short (~6.8 nm) that the hydrogen bonding is pronounced. We believe that strong intermicrogel hydrogen bonding exists in the microgel−microgel overpacked regions, and likewise, as packing density decreases, they will be weakened. Hence, in pH 3.0 solution, the etalon has to overcome microgel−Au interactions and microgel−microgel interactions to swell,

Scheme 2. Cartoon Illustrating the Structure and Thickness Change of an Etalon Painted at Different pH/I.S., and the Microgel–Au and Microgel–Microgel Interactions

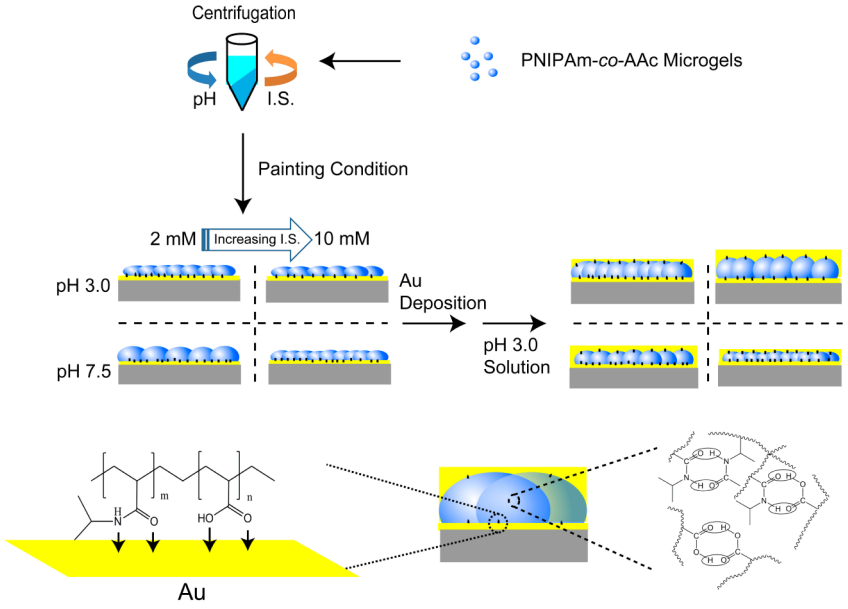

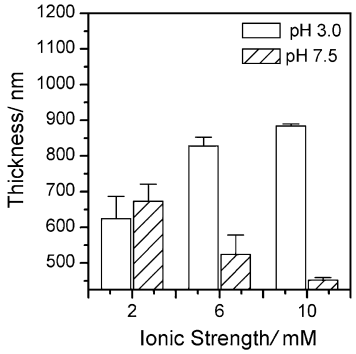

Figure 4. Etalon thickness as a function of microgel deposition solution pH and I.S. The thickness was averaged from five random regions in an AFM image.

both of which depend on the packing density. In the context of painting at pH 3.0, the packing density is decreased with increasing I.S., resulting in the weakening of both interactions. Therefore, the microgel layer easily swells, yielding a thicker film with increasing I.S. (Scheme 2).

However, the thickness of the etalon is decreased with increasing painting I.S., when painting at pH 7.5 (Scheme 2 and Figure 4). Again, when the etalon is immersed in pH 3.0 solution, the swelling of the etalon is influenced by the microgel–Au interactions and microgel–microgel interactions, both of which are based on the packing density. As discussed previously, the particle number density is increased with increasing painting I.S. (Figure 3). Therefore, after the etalon is immersed at pH 3.0, the swelling behaviour is frustrated due to stronger microgel–microgel hydrogen bonding between neighboring particles as well as the enhanced microgel–Au interactions. As a result, the thickness of the etalon is decreased from 673 ± 48 nm (painting solution I.S. 2 mM), to 524 ± 54 nm (painting solution I.S. 6 mM), and to 452 ± 7 nm (painting solution I.S. 10 mM).

Optical Properties of the Etalon in pH 3.0 Solution. Understanding the morphology and thickness of the etalon, we further studied how the deposition conditions affected optical properties of etalons to sense solution pH. As seen in Figure 5, we measured a reflectance spectrum from 10 random spots of each etalon and indicate the average peak position and standard deviation. We note that the position of the samples in the thermal evaprator does not affect the optical properties of the etalon (see the Supporting Information). Reflectance spectra can be obtained from etalons in all cases, illustrating that the painting protocol can yield an etalon in all cases. To further elucidate different optical properties, we compare the λ_3 (λ at peak order m = 3, which was calculated by eq 1) in the spectrum as a function of painting pH and I.S. As shown in Figure 5, the λ_3 is 760 ± 15 nm (I.S. 2 mM), 821 ± 16 nm (I.S. 6 mM), and 820 ± 16 nm (I.S. 10 mM). These standard deviations are smaller than the etalons constructed from microgels painted in DI water,[15] showing an enhanced homogeneity of the etalon. However, when painting at pH 7.5 with an I.S. of 2 mM, λ_3 = 780 ± 39 nm. This larger standard deviation is indicative of much different optical properties among these random spots on the etalon. With increasing I.S., packing density is increased; therefore, we expect that a macroscopic, homogeneous, and integral thin microgel film is more easily obtained. Hence, the behavior of the microgel-based etalon is more like an ideal Fabry–Pérot etalon, producing homogeneous optical signals from different regions on the device (Scheme 3; more details can be seen in the Supporting Information). For example, when painting at pH 7.5 with an I.S. of 10 mM, λ_3 = 649 ± 12 nm.

Sensitivity of the Etalon to Solution pH Changes. Finally, the effect of painting conditions on the etalon sensitivity to pH changes was investigated. Etalons were first rinsed with DI water, dried under N_2 gas, and immersed in pH 6.5 (2 mM I.S.) solution overnight. Then, we also measured the reflectance spectrum of each etalon at 10 random regions at 25 °C, and compared the position of λ_3 at pH 3.0 and 6.5. We then calculated the difference of the peak position as an indication of the etalon sensitivity to pH: $\Delta\lambda_3 = \lambda_3$ (at pH 6.5) − λ_3 (at pH 3.0). When etalons are immersed in pH 6.5 solution, $\Delta\lambda_3 > 0$ in all cases, showing λ_3 red shifts (Figure 6). Microgel monolayer

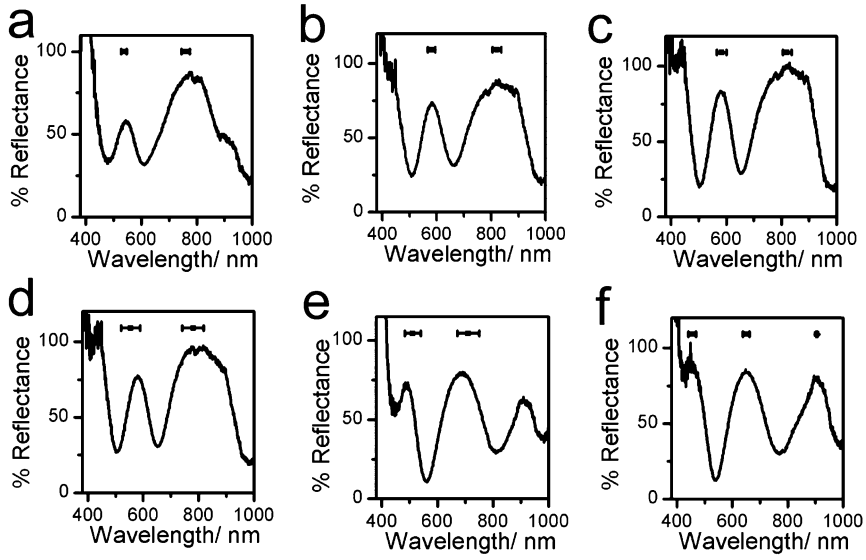

Figure 5. Representative reflectance spectra of etalons as a function of microgel deposition solution pH and I.S.: (a) pH 3.0, I.S. 2 mM, (b) pH 3.0, I.S. 6 mM, (c) pH 3.0, I.S. 10 mM, (d) pH 7.5, I.S. 2 mM, (e) pH 7.5, I.S. 6 mM, and (f) pH 7.5, I.S. 10 mM. Etalons were immersed in pH 3.0, I.S. 2 mM solution at 25 °C. The point above each peak is the average peak position for 10 random spots on the etalon with the error bars indicative of the standard deviation of the peak position.

Scheme 3. A Proposed Mechanism for How Packing Density Affects the Optical Homogeneity of the Etalon

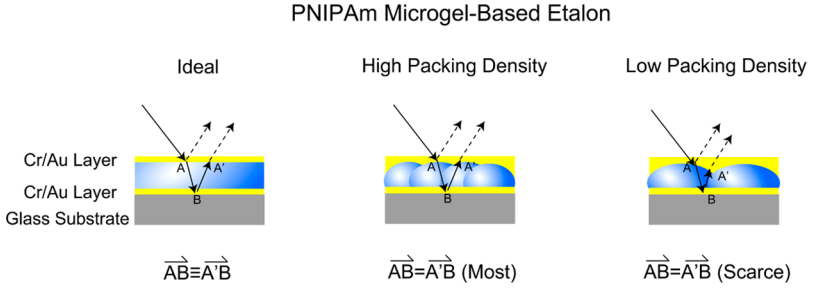

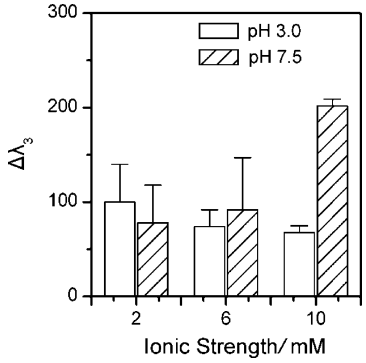

Figure 6. $\Delta\lambda_3$ from pH 3.0 to pH 6.5 as a function of microgel deposition solution pH and I.S.

swelling is definitely driven by the electrostatic repulsion in a sole microgel, while it can be also largely enhanced by the neighboring particles, or negative charges in the overpacking region. Namely, electrostatic repulsion at higher packing density should have a greater influence on microgel monolayer swelling. Meanwhile, the swelling is more or less hampered due to the microgel−Au interactions. The trend in Figure 6 implies that, when painting at pH 3.0 with an increasing I.S., the packing density is decreased and, therefore, the response to pH is diminished. Conversely, in the case of painting at pH 7.5, packing density is increased with increasing painting I.S. Albeit the microgel−Au interactions are stronger for higher painting I.S., the enhanced electrostatic repulsion among the microgels favors the monolayer swelling, yielding an increase in pH response and hence a greater $\Delta\lambda_3$. Therefore, the thinnest microgel thin film (painted at pH 7.5, 10 mM) gives the highest response to pH changes from pH 3.0 to pH 6.5.

CONCLUSIONS

We have demonstrated that pNIPAm-*co*-AAc microgels are responsive to solution pH and I.S., exhibiting various hydrodynamic diameters. A series of pNIPAm-*co*-AAc microgel-based thin films and etalons were fabricated via painting different microgel deposition solutions on a Au-coated substrate, followed by deposition of another Au overlayer. It is shown that the deposition solution pH and I.S. influence the microgel assembly, which impacts optical homogeneity and ultimately the pH sensitivity of the etalon.

ASSOCIATED CONTENT

Supporting Information

The center-to-center distance (D_C) of adjacent microgels, the microgel apparent diameter (D) on the Au-coated substrate, differential interference contrast microscope images for the etalons, AFM cross-sectional images and corresponding analyses for the etalons, reflectance spectra of an etalon

measured at five random spots in DI water, the discussion of Scheme 3, and the LCST curve for the pNIPAm-*co*-AAc microgels. This material is available free of charge via the Internet at http://pubs.acs.org.

AUTHOR INFORMATION

Corresponding Author

*E-mail: michael.serpe@ualberta.ca.

Notes

The authors declare no competing financial interest.

ACKNOWLEDGMENTS

M.J.S. acknowledges funding from the University of Alberta (the Department of Chemistry and the Faculty of Science), the Natural Science and Engineering Research Council (NSERC), the Canada Foundation for Innovation (CFI), the Alberta Advanced Education & Technology Small Equipment Grants Program (AET/SEGP), and Grand Challenges Canada. M.J.S. acknowledges Mark McDermott for the use of the thermal evaporator. L.H. would like to thank the China Scholarship Council (CSC) for financial support.

REFERENCES

(1) Saunders, B. R.; Vincent, B. *Adv. Colloid Interface Sci.* **1999**, *80*, 1−25.
(2) Oh, J. K.; Drumright, R.; Siegwart, D. J.; Matyjaszewski, K. *Prog. Polym. Sci.* **2008**, *33*, 448−477.
(3) Lyon, L. A.; Meng, Z.; Singh, N.; Sorrell, C. D.; John, A. S. *Chem. Soc. Rev.* **2009**, *38*, 865−874.
(4) Karg, M.; Hellweg, T. *Curr. Opin. Colloid Interface Sci.* **2009**, *14*, 438−450.
(5) Ballauff, M.; Lu, Y. *Polymer* **2007**, *48*, 1815−1823.
(6) Quesada-Perez, M.; Alberto Maroto-Centeno, J.; Forcada, J.; Hidalgo-Alvarez, R. *Soft Matter* **2011**, *7*, 10536−10547.
(7) Fernandez-Nieves, A.; Fernandez-Barbero, A.; Vincent, B.; de las Nieves, F. J. *Macromolecules* **2000**, *33*, 2114−2118.
(8) Hoare, T.; Pelton, R. *Macromolecules* **2004**, *37*, 2544−2550.
(9) Nolan, C. M.; Serpe, M. J.; Lyon, L. A. *Biomacromolecules* **2004**, *5*, 1940−1946.
(10) Senff, H.; Richtering, W. *J. Chem. Phys.* **1999**, *111*, 1705−1711.
(11) Kratz, K.; Hellweg, T.; Eimer, W. *Colloids Surf., A* **2000**, *170*, 137−149.
(12) Snowden, M. J.; Chowdhry, B. Z.; Vincent, B.; Morris, G. E. *J. Chem. Soc., Faraday Trans.* **1996**, *92*, 5013−5016.
(13) Gan, T. T.; Zhang, Y. J.; Guan, Y. *Biomacromolecules* **2009**, *10*, 1410−1415.
(14) Lapeyre, V.; Gosse, I.; Chevreux, S.; Ravaine, V. *Biomacromolecules* **2006**, *7*, 3356−3363.
(15) Hu, L.; Serpe, M. J. *J. Mater. Chem.* **2012**, *22*, 8199−8202.
(16) Nolan, C. M.; Reyes, C. D.; Debord, J. D.; García, A. J.; Lyon, L. A. *Biomacromolecules* **2005**, *6*, 2032−2039.
(17) Singh, N.; Bridges, A. W.; Garcia, A. J.; Lyon, L. A. *Biomacromolecules* **2007**, *8*, 3271−3275.
(18) Schmidt, S.; Zeiser, M.; Hellweg, T.; Duschl, C.; Fery, A.; Mohwald, H. *Adv. Funct. Mater.* **2010**, *20*, 3235−3243.
(19) Liu, P.; Luo, Q.; Guan, Y.; Zhang, Y. *Polymer* **2010**, *51*, 2668−2675.
(20) Lynch, I.; de Gregorio, P.; Dawson, K. A. *J. Phys. Chem. B* **2005**, *109*, 6257−6261.
(21) Parasuraman, D.; Serpe, M. J. *ACS Appl. Mater. Interfaces* **2011**, *3*, 4714−4721.
(22) Parasuraman, D.; Serpe, M. J. *ACS Appl. Mater. Interfaces* **2011**, *3*, 2732−2737.
(23) Sorrell, C. D.; Carter, M. C. D.; Serpe, M. J. *Adv. Funct. Mater.* **2011**, *21*, 425−433.
(24) Kim, J.; Serpe, M. J.; Lyon, L. A. *Angew. Chem., Int. Ed.* **2005**, *44*, 1333−1336.
(25) Sakai, T.; Takeoka, Y.; Seki, T.; Yoshida, R. *Langmuir* **2007**, *23*, 8651−8654.
(26) Heppner, I.; Serpe, M. *Colloid Polym. Sci.* **2013**, *291*, 1−6.
(27) Sorrell, C. D.; Serpe, M. J. *Anal. Bioanal. Chem.* **2012**, *402*, 2385−2393.
(28) Islam, M. R.; Serpe, M. J. *Macromolecules* **2013**, *46*, 1599−1606.
(29) Islam, M. R.; Serpe, M. J. *Chem. Commun.* **2013**, *49*, 2646−2648.
(30) Johnson, K. C. C.; Mendez, F.; Serpe, M. J. *Anal. Chim. Acta* **2012**, *739*, 83−88.
(31) Sorrell, C. D.; Carter, M. C. D.; Serpe, M. J. *ACS Appl. Mater. Interfaces* **2011**, *3*, 1140−1147.
(32) Burmistrova, A.; von Klitzing, R. *J. Mater. Chem.* **2010**, *20*, 3502−3507.
(33) Debord, S. B.; Lyon, L. A. *J. Phys. Chem. B* **2003**, *107*, 2927−2932.
(34) Heyes, D. M.; Branka, A. C. *Soft Matter* **2009**, *5*, 2681−2685.
(35) Lyon, L. A.; Debord, J. D.; Debord, S. B.; Jones, C. D.; McGrath, J. G.; Serpe, M. J. *J. Phys. Chem. B* **2004**, *108*, 19099−19108.
(36) St. John, A. N.; Breedveld, V.; Lyon, L. A. *J. Phys. Chem. B* **2007**, *111*, 7796−7801.
(37) Trappe, V.; Prasad, V.; Cipelletti, L.; Segre, P. N.; Weitz, D. A. *Nature* **2001**, *411*, 772−775.
(38) Meng, Z.; Cho, J. K.; Breedveld, V.; Lyon, L. A. *J. Phys. Chem. B* **2009**, *113*, 4590−4599.
(39) Meng, Z.; Cho, J. K.; Debord, S.; Breedveld, V.; Lyon, L. A. *J. Phys. Chem. B* **2007**, *111*, 6992−6997.
(40) Lu, Y.; Drechsler, M. *Langmuir* **2009**, *25*, 13100−13105.
(41) Nerapusri, V.; Keddie, J. L.; Vincent, B.; Bushnak, I. A. *Langmuir* **2006**, *22*, 5036−5041.
(42) Iori, F.; Corni, S.; Di Felice, R. *J. Phys. Chem. C* **2008**, *112*, 13540−13545.
(43) Bilic, A.; Reimers, J. R.; Hush, N. S.; Hafner, J. *J. Chem. Phys.* **2002**, *116*, 8981−8987.